ACS Sustainable Chemistry & Engineering

Research Article

pubs.acs.org/journal/ascecg

Conversion of Lignin Precursors to Carbon Fibers with Nanoscale Graphitic Domains

Sabornie Chatterjee,*[,†] Eric B. Jones,[‡] Amy C. Clingenpeel,[§] Amy M. McKenna,[∥] Orlando Rios,[‡] Nicholas W. McNutt,[⊥] David J. Keffer,[#] and Alexander Johs*[,†]

[†]Environmental Sciences Division and [‡]Materials Science & Technology Division, Oak Ridge National Laboratory, 1 Bethel Valley Road, Oak Ridge, Tennessee 37831, United States

[§]Department of Chemistry and Biochemistry, 95 Chieftain Way, Florida State University, Tallahassee, Florida 32304, United States

[∥]National High Magnetic Field Laboratory, Florida State University, 1800 East Paul Dirac Drive, Tallahassee, Florida 32310, United States

[⊥]Department of Chemical & Biomolecular Engineering and [#]Department of Materials Science & Engineering, University of Tennessee, Knoxville, Tennessee 37996, United States

ABSTRACT: Lignin is one of the most abundant and inexpensive natural biopolymers. It can be efficiently converted to low cost carbon fiber, monolithic structures, or powders that could be used directly in the production of anodes for lithium-ion batteries. In this work, we report thermomechanical processing methods relevant for the conversion of lignin precursors into carbon fiber-based anode materials, the impact of lignin precursor modification on melt processing, and the microstructure of the final carbon material. Modification of softwood lignin produced functionalities and rheological properties that more closely resemble hardwood lignin thereby enabling the melt processing of softwood lignin in oxidative atmospheres (air). The conversion process encompasses melt spinning of the lignin precursor, oxidative stabilization, and a low temperature carbonization step in a nitrogen/hydrogen atmosphere. We determined resistivities of individual carbon fiber samples and characterized the microstructure by scanning electron microscopy. Neutron diffraction reveals nanoscale graphitic domains embedded in an amorphous carbon matrix. These unique structural characteristics make biomass-derived carbon fibers a suitable material for energy storage applications with enhanced electrochemical performance.

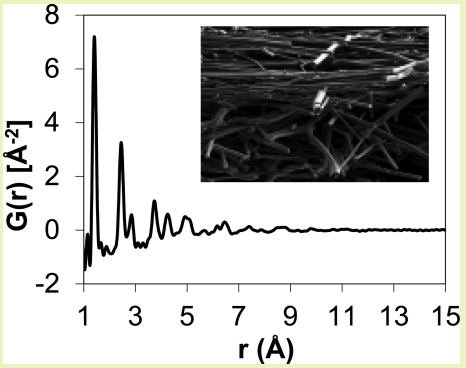

KEYWORDS: *Lignin, Carbon fibers, Carbon materials, Fourier-transform ion cyclotron resonance, Neutron scattering*

INTRODUCTION

Carbon fiber, an emerging engineered material, generally used in the manufacturing of advanced composites[1,2] has various applications in the automotive, aerospace, and electronics industry. Since its widespread commercialization in the 1960s, pitch, derived from petroleum or coal, and polyacrylonitrile are the most common types of precursor materials used to produce carbon fiber commercially. Almost 80% of commercial carbon fiber is estimated to use PAN (polyacrylonitrile) as a precursor. PAN is a linear polymer derived from petroleum. Linear PAN contains polar nitrile groups that result in strong intermolecular interactions, which results in carbon fibers with excellent mechanical properties. However, carbon fiber produced from PAN is expensive and thus its application is limited to high-performance structural materials.

Lignin is a carbon-rich renewable resource and the second most abundant biopolymer in nature after cellulose.[3,4] As a byproduct of the pulp and paper industry and the production of cellulosic ethanol, lignin is available at low cost making it an economically attractive alternative to PAN for the production of carbon fibers. Unlike PAN-based fibers, which usually require wet- or dry-spinning using highly polar solvents, lignin fibers are generally synthesized by melt-spinning followed by oxidative stabilization and carbonization. While wet- and dry-spinning involve dissolution of the precursor into a solvent and then extrusion into either a coagulation bath (wet spinning) or a drying chamber (dry spinning), where the polymer precipitates into fiber form, melt spinning merely requires that the polymer be fed into a heated extruder where it is melted and then pushed through a spinneret nozzle, or die.[5,6] Most lignins can be directly processed by melt spinning, because their melting temperature is well below the oxidation temperature.[6,7] PAN, on the other hand, due to its high intermolecular interactions, has a high melting point and tends to degrade before it melts, thus rendering it incompatible with the melt spinning process. This clearly makes lignin a desirable precursor, as the melt spinning process is unburdened by the

Received: March 16, 2014
Revised: June 1, 2014
Published: June 24, 2014

   dx.doi.org/10.1021/sc500189p | ACS Sustainable Chem. Eng. 2014, 2, 2002−2010

solvent procurement and recovery issues associated with wet- and dry-spinning.

Unfortunately, lignin carbon fibers have inferior mechanical properties that generally limit their use in structural applications. Interestingly, lignin-based carbons show great potential for energy storage applications such as lithium ion batteries or supercapacitors. Conventional lithium-ion batteries are costly and time-consuming to fabricate. For example, the price of copper alone, which is a widely used current collector in anodes, currently hovers around $3.30/lb[8] and the full cost for raw materials for a copper-graphite anode is around $16.00/lb. Thus, in order to minimize both the environmental and economic impacts of battery production and use, it is essential to develop streamlined manufacturing methods that maximize the use of renewable materials. The most commonly used anode material for Li-ion batteries is graphite, which can insert lithium reversibly. Graphite as an electrode material has some drawbacks, such as limited stability due to its structure, low capacity, and high sensitivity to electrolyte solutions.[9] Reaction of graphite with electrolyte solutions results in the formation of surface coatings on graphite anodes which results in capacity loss and battery failure. The use of high porosity carbon anode materials increases the robustness of the electrode;[9−13] however, the large surface area leads to extensive binding of Li-ions in the solid electrolyte interface.[14−16] Several processes to obtain microstructured carbons that behave more robust during repeated lithium (Li) ion insertion and deinsertion in a wide spectrum of electrolytic solutions have been reported in the literature. Examples include the use of chemical vapor deposited carbon cloth,[9] preparation of disordered carbon materials by gas phase reaction of liquid propane gas,[10] use of mesophase pitch based carbon fibers,[11] pretreatment with gelatin,[12] etc. However, most of these methods are complex, require expensive chemicals and are therefore not economically viable. Recent reports indicate that lignin based low-cost carbons are promising materials for current Li-ion battery technologies and future Na-ion chemistries because of lignin's unique carbon microstructure with a high degree of turbostratic disorder.[17,18]

There are a few challenges in making lignin based carbon fibers for energy storage applications. Lignin is a three-dimensional branched copolymer which is randomly bridged in nature. Lignin consists of three basic monomeric units or monolignols which are *p*-coumaryl (H), coniferyl (G), and sinapyl (S) alcohols. The relative distributions of these monomeric units in any lignin sample depend on the plant source. For example, the S/G ratios in hardwood and softwood lignins are 2:1 and 1:2−1:3, respectively. Thus, the natural inhomogeneity of lignin must be considered before using it in a particular process such as conversion to carbon fibers. Additionally, commercial lignins, such as those isolated from alkaline, acidic or organic solvent-based processes have undergone extensive fragmentation and degradation.[6,19] As a result, lignins with variable chemical properties and structures are obtained. Also, most industrial lignins contain significant amounts of impurities, which may lead to inconsistent rheological properties that hinder the application of scalable methods of producing carbon fibers from melt processing and subsequent thermal conversion.[8,20,21] These difficulties can be overcome by pretreatment of raw lignins. Solvent extraction and chemical modification have been successfully used to obtain standardized preparations of lignin precursors.[18] The chemical composition and structure of the lignin precursors determine the characteristics during melt processing and microstructure development during carbonization. For example, the level of turbostratic disorder of the lignin carbon fiber can be controlled by adjusting the temperature during carbonization.[8,22,23] Also, the macroscopic properties and morphology of lignin carbon fibers can be tuned by adjusting thermal profile and processing conditions. As an example heating of lignin fiber mats near the glass transition temperature (T_g) during oxidative stabilization results in controllable degrees of fiber−fiber fusion to produce a three dimensionally interconnected monolithic structure.[22] The result is a cross-linked lignin carbon fiber mat architecture, which eliminates the need for binders, conductive additives and a current collector as the fused carbon fiber mat serves as active material and current collector simultaneously, potentially simplifying the production of Li-ion or Na-ion batteries.

Described in this manuscript is a process for the conversion of solvent-extracted Alcell hardwood and Kraft softwood lignins into biomass-derived carbon fibers with a morphology optimized for advanced energy storage applications, such as anode materials for lithium or sodium ion batteries.

EXPERIMENTAL SECTION

Materials. The lignin types used in this study were solvent extracted Alcell hardwood lignin and Kraft softwood lignin. All lignin samples were dried under vacuum at 80 °C for 48 h before use. All other chemicals and reagents including acid anhydrides (acetic, succinic, phthalic, and maleic) and solvents such as tetrahydrofuran (THF) and methanol (MeOH) for chemical modification were purchased from Sigma-Aldrich, USA, and used as received.

Chemical Modification of Lignin Precursors. The chemical modification of lignin precursor used in this work has been described previously.[18] Briefly, commercially available Alcell hardwood lignin (AHL) and Kraft softwood lignin (KSL) were used as the precursors for chemical modifications. The specific acid anhydrides used to react with AHL hydroxyl groups were acetic anhydride, phthalic anhydride, maleic anhydride, and succinic anhydride. Phthalic anhydride and acetic anhydride modified softwood lignins were tested as well.

Analysis of Lignin Precursors. Fourier transform ion cyclotron resonance mass spectrometry (FT-ICR MS) is an ultrahigh resolution mass spectrometry method that enables analysis of complex mixtures such as natural biopolymers. Lignin samples were dissolved in THF, to yield a 1 mg/mL stock solution. Stock solutions were further diluted to a final concentration of 250 μg/mL in 50:50 (MeOH:THF) with 1% (by volume) ammonium hydroxide (NH_4OH) for negative electrospray ionization (ESI) prior to FT-ICR mass spectral analysis.[24] FT-ICR MS analyses were performed on a custom built FT-ICR mass spectrometer coupled to a room temperature 9.4 T superconducting magnet (Oxford, U.K)[25] at the National High Magnetic Field Lab, Tallahassee, FL. Data acquisition was done with a modular ICR data station (PREDATOR).[26] Multiple (100) individual time-domain transients were coadded, Hanning-apodized, zero-filled, and fast Fourier transformed prior to frequency conversion to mass-to-charge ratios to obtain the final mass spectrum.[27] Peak lists were generated with custom-built software (MIDAS) for all peaks with signal magnitude greater than six times the baseline RMS noise. The spectra were internally calibrated based on the "walking" calibration[28] with the highly abundant homologous O_2 series, which differ in mass by 14.01565 Da (mass of a CH_2 unit). IUPAC mass can be converted to Kendrick mass (Kendrick mass = IUPAC mass × (14/14.01565)) to facilitate rapid identification of compounds that differ in mass by 14 Da.[29] Compounds with the same heteroatom content (nitrogen, oxygen, sulfur) but differ by degree of alkylation are grouped together for rapid identification of homologous series.[30]

Optimization of Extrusion Parameters. A Dynisco laboratory mixing extruder (LME) and take-up system (TUS) were used in order to optimize six fiber spinning parameters for Alcell hardwood lignin

(AHL): rotor temperature, header temperature, rotor speed, TUS reel speed, axial gap clearance, and hopper ramming method (Table 1).

Table 1. Optimized Extrusion Parameters for Unmodified Alcell Hardwood Lignin (AHL)

	rotor temp (°C)	header temp (°C)	rotor speed (Hz)	TUS reel speed (ft/s)	axial gap clearence (in)	ramming method
optimal setting	175	200	0.6	1.5	0.005	dense packing

The viscous melt temperature (T_m) of AHL (160 °C) was first determined by heating in a laboratory oven. The rotor temperature was fixed at this temperature while the header temperature was varied from 160 to 210 °C in increments of 5 °C, allowing 15 min for equilibration before samples were taken. During this process, the following parameters were fixed: rotor speed 3.8 Hz, TUS reel speed maximum (1.5 ft/s), axial gap clearance 0.020 in., and hopper ramming method dense packing. Once 200 °C was determined, and thus fixed, as the optimal header temperature, the rotor temperature was varied from 160 to 200 °C by the same method, with all other parameters fixed as before. The rotor temperature was then set to 175 °C. The other four parameters were then optimized by varying them as follows: rotor speed 0−100% of maximum (0−4.6 Hz), TUS reel speed 6−maximum (0.6−1.5 ft/s), axial gap clearance 0.005−0.020 in., and hopper ramming method dense packing and self-loading. The optimal parameters were determined to be the following: rotor temperature 175 °C, header temperature 200 °C, rotor speed 0.6 Hz, TUS reel speed maximum (1.5 ft/s), axial gap clearance 0.005 in., and hopper ramming method dense packing.

Extrusion of Modified Lignin Precursors. After a baseline set of optimal spinning parameters was determined, fiber extrusion and uptake were initiated for modified lignin precursor samples. Extrusion of modified precursors was performed using sample sizes of 6−8 g. Single strands, ranging in length from 4 to 10 in were arranged parallel to one another in preparation for thermostabilization and carbonization. All modified samples were spun using the optimized parameters for unmodified AHL, adjusting temperature as necessary in order to accommodate the varying chemical composition of different samples. Spinning temperatures for modified lignins are given in Table 2. Thermostabilization and carbonization: Spun fibers were

Table 2. Extrusion Parameters for Modified Lignins

sample	rotor (°C)	header (°C)
acetic anhydride modified AHL	175	198
phthalic anhydride modified AHL	175	200
maleic anhydride modified AHL	175−235	210−255
succinic anhydride modified AHL	180	205
acetic anhydride modified KSL	195	220
phthalic anhydride modified KSL	210	230

arranged in a cross-hatched pattern on aluminum foil in order to achieve fiber−fiber fusion during thermostabilization. The fibers were then placed in a laboratory convection oven, which was heated from 21 to 249 °C at heating rates of less than 3 °C/min. Thermostabilization was performed in air. Samples were then carbonized at 1000 °C for 30 min in an atmosphere of 96% argon and 4% hydrogen.

Neutron Diffraction Experiments. In order to characterize the atomic structure of the carbon fibers, neutron diffraction data of unmodified and modified samples was collected on the Nanoscale-Ordered Materials Diffractometer (NOMAD) of the Spallation Neutron Source (SNS) at Oak Ridge National Laboratory (ORNL), Oak Ridge, TN.

Scanning Electron Microscopy. The structural characteristics and dimensions of carbon fibers were evaluated using scanning electron microscopy (SEM) using a JEOL 6500F scanning electron microscope in secondary electron imaging mode with a 10 keV accelerating voltage.

Resistivity Measurements. A Signametrics multimeter was used to measure the resistance of lignin carbon fibers by a four-terminal sensing scheme. Single carbon fibers were placed on a glass slide with four lines of conductive carbon paint leading from the fibers to the edge of the slide. Two leads were connected to the outside lines, forcing a current through the length of the fiber. The voltage drop around the center of each of the fibers was measured using leads connected to the inner two lines. From the voltage differential and current, the multimeter calculated the resistance of each fiber, while eliminating contributions due to contact resistance. The distances between the innermost leads were measured and fiber diameters were obtained from SEM images and the average resistivity was calculated for each type of fiber.

RESULTS AND DISCUSSION

Characterization of Lignin Precursors by FT-ICR MS. The very high accuracy mass determination combined with electrospray ionization (ESI) offers sufficient sensitivity to detect changes in the lignin backbone structure as well as differences in functional groups as a result of esterification reactions.[18] The mass spectra for AHL and KSL reveal a total of ~9000 and ~7000 distinct peaks, respectively (Figure 1).

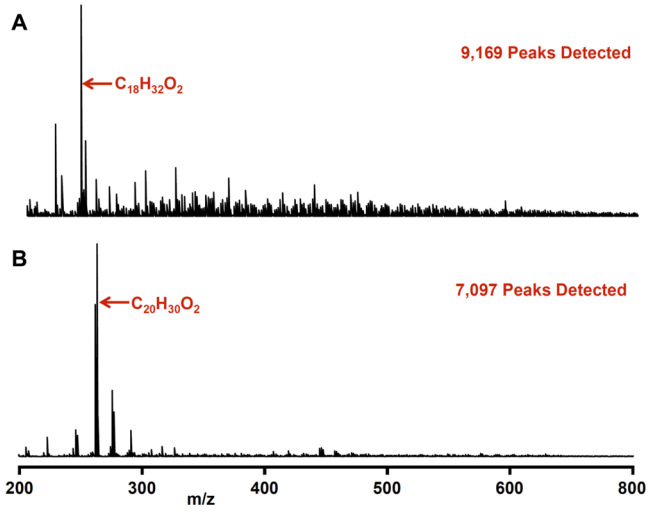

Figure 1. Negative ion ESI FT-ICR (9.4 T) mass spectra of (A) hardwood Alcell lignin and (B) softwood Kraft lignin. Peaks with signal magnitudes greater than six times the baseline RMS noise were assigned to heteroatom classes.

However, both spectra show a limited number of characteristic peaks with high abundance. The mass to charge ratio (m/z) for the highest abundance peak in the mass spectrum for AHL corresponds to $C_{18}H_{32}O_2$, while the m/z for the highest abundance peak in the mass spectrum for KSL corresponds to $C_{20}H_{30}O_2$. The heteroatom class graphs show distinct class compositions for AHL and KSL samples (Figure 2). While the heteroatom class O_8 represents the maximum relative abundance for AHL at 5%, O_2 was the highest abundance class for KSL at 24%. Modification with phthalic anhydride resulted in an overall shift to higher molecular weight classes. Interestingly, the esterification of KSL with phthalic anhydride results in a heteroatom class distribution more closely resembling AHL.

Previously, FT-ICR-MS of steam-exploded wheat straw and bagasse lignins were reported to show some regularity with difference of 44.026 m/z between the mass peaks.[31,32] The

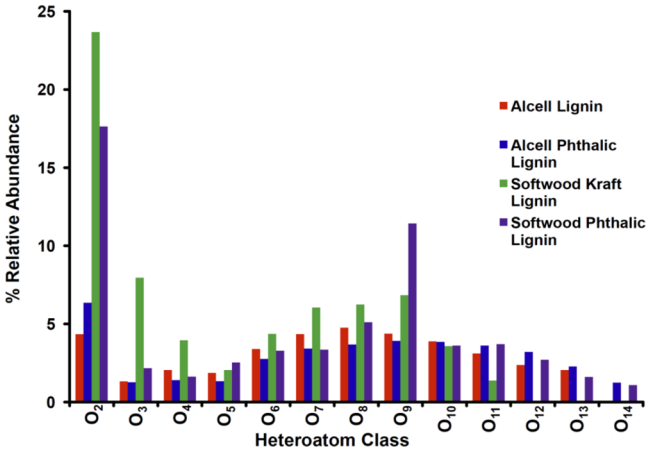

Figure 2. Heteroatom class distributions for unmodified and modified hardwood and softwood lignins.

authors reported that Kendrick mass plots of all lignin samples showed some correlated slopes. All these observations indicated the presence of some homogeneity in the used lignin. In our work, no correlation was found between peaks in the mass fragmentation pattern of organosolv lignin samples.

Van Krevelen diagrams plot the molar ratio of hydrogen to carbon (H:C) versus the molar ratio of oxygen to carbon (O:C) and have been applied extensively to study complex organic samples such as natural organic matter.[33] The H:C ratio increases as the number of rings plus double bonds decreases, while the O:C ratio distinguishes heteroatom classes based on the number of O atoms. Because major chemical compound classes, such as lipids, carbohydrates, and lignin, have characteristic H:C or O:C ratios, van Krevelen diagrams provide rapid identification of compound classes and help in identifying changes in the chemical composition based on the distribution of peaks in the plot. Elemental compositions for each peak calculated from negative-ion ESI FT-ICR mass spectra provide H:C and O:C ratios for modified and unmodified AHL and KSL (Figure 3). The H:C range for AHL (0.65−1.39) was lower than the range for KSL (0.76−1.47) while the range of O:C ratios were identical (0.15−0.49). The esterification of AHL with phthalic anhydride results in a negligible change in the range of H:C ratios (0.65−1.38). However, phthalic anhydride modification of KSL had a significant impact on both ranges, H:C (0.76−1.38) and O:C (0.15−0.43).

Conversion of Lignin to Carbon Fibers. The indicator as to whether or not a particular set of spinning parameters yielded an optimally spinnable extrusion was whether or not fibers, with a diameter of ∼40 μm, could be wound continuously to a length of 4.57 m on the TUS. While Kadla et al.[34] report spinning Alcell hardwood lignin at 138−165 °C

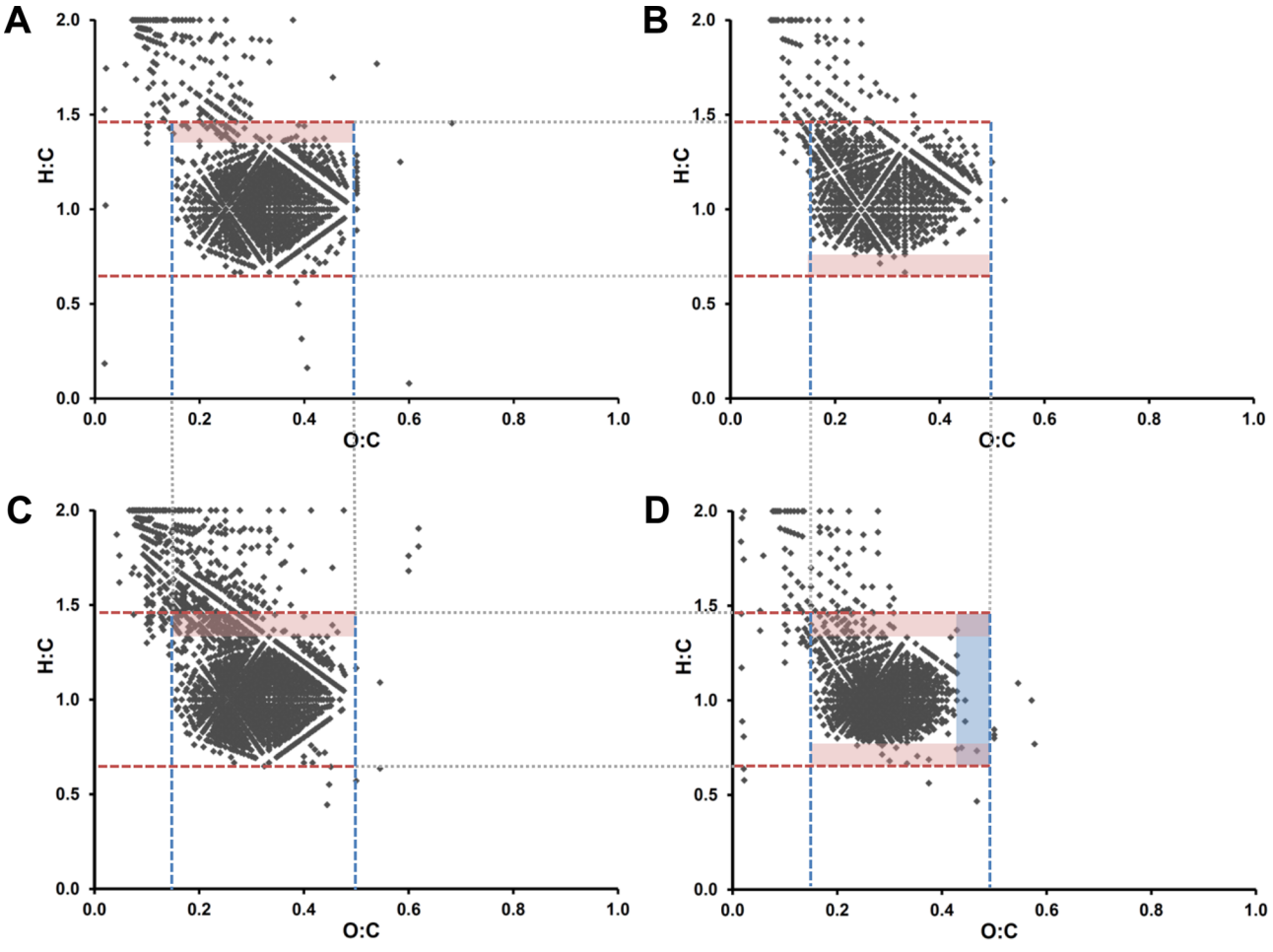

Figure 3. Van Krevelen plots for (A) AHL, (B) KSL, (C) phthalic anhydride modified AHL, and (D) phthalic anhydride modified KSL obtained from the assigned elemental composition for each peak in the mass spectrum.

and Luo[35] reports spinning temperatures in the range 145−170 °C, for the same Alcell hardwood lignin, we found that the optimal spinning temperatures were 175 °C at the rotor and 200 °C at the header. These higher temperatures resulted in a lower viscosity extrusion through the spinneret nozzle and thus one, which could be taken up with sufficient speed to create fine, continuously spinnable, and flexible fibers. By contrast, in the 145−170 °C temperature range, Luo comments that Alcell fibers are "still brittle",[35] consistent with observations in the present study. Significant deviation from the optimal spinning temperatures toward cooler temperatures results in an overly viscous extrusion, which results in brittle, nonspinnable fibers. Meanwhile, deviation toward higher temperatures results in runaway extrusion, oxidation, and lignin charring.

Another important quantity, as it pertains to LME temperature settings, is the difference between the rotor and header temperatures. In part, the extrusion process is governed by the pressure gradient inside the extruder, which in turn is governed by the temperature gradient between the rotor and the header regions. Too low a gradient results in weak, irregular extrusion whereas too high a gradient results in runaway extrusion. The 25 °C difference produced a controlled, yet sufficiently rapid extrusion.

The optimal rotor frequency was determined to be 0.6 Hz. This was the lowest frequency at which sufficient mixing of lignin occurred, while still allowing a primarily pressure-driven extrusion process. At higher frequencies, the mechanical contribution to the extrusion process introduced vapor nonuniformities and resulted in thicker fibers with higher incidence of breakage. Similarly, the axial gap clearance was set to 0.005 in., the smallest possible clearance before instability-induced grinding occurred between the rotor face and the header, in order to mitigate such effects. The TUS spool was set to its maximum speed, 1.5 ft/s, in order to produce the finest fibers possible.

Finally, it became apparent that the method by which lignin is fed into the LME hopper significantly impacts the quality of the resulting extrusion. Although more common and easy-to-process polymers such as polypropylene and polystyrene can be self-fed into the extruder, raw AHL requires manual loading with a ramming implement. This is both because melted AHL has a tendency to migrate back up the hopper chute, solidify and prevent further loading, and because it readily carries vapor nonuniformities with it to the spinneret nozzle, which causes breakage during fiber uptake. Thus, manual loading is used to firmly pack the hopper, creating a region of dense lignin composition, which when transported through the extruder results in a continuous, uniform extrusion. This firm ramming method is another reason that the axial gap clearance and the rotor frequency were set low, as the region of high density contributes significantly to the pressure gradient inside the LME.

Modified Precursor Extrusion. Reaction of acid anhydrides with accessible hydroxyl groups on the lignin polymer backbone has a significant influence on the melt processability. The former is affected by the degree to which carboxyl and carbonyl functional groups are introduced to the precursor via modification. During carbonization, these functional groups then volatilize, resulting in a controllable degree of microscale porosity (Figure 4). Meanwhile, the latter advantage of modification is that it prevents charring due to decreased cross-linking of the polymer, which reduces the melting temperature of the lignin and thus, its viscosity during

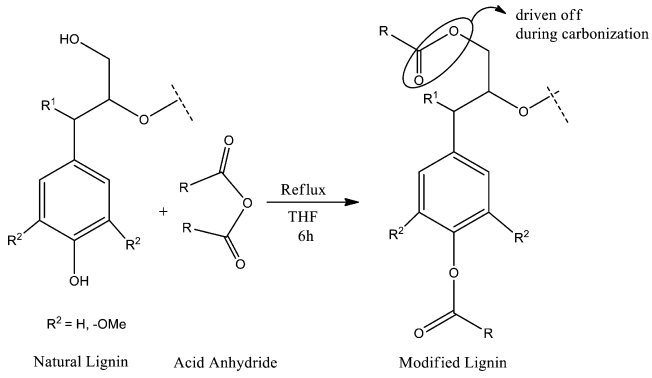

Figure 4. Chemistry of lignin modification.

extrusion. However, certain modifications seem to have actually increased cross-linking, inducing an unspinnable extrusion, which oxidizes before a fluid flow can be achieved. There is evidence that both acetic anhydride and phthalic anhydride succeed in reducing polymeric cross-linking AHL. Acetic anhydride was spun at 175/198 °C and phthalic at 175/200 °C. At these temperatures, which are optimal for raw AHL, the extrusion was by far more fluid, requiring much less pressure to be present behind the spinneret nozzle. Although these extrusions were able to be taken up on the TUS, they were principally drawn by hand to form fine, flexible fibers. By contrast, the succinic and maleic modifications rendered viscous extrusions at both identical and higher temperatures. Furthermore, the maleic anhydride modification caused oxidation beginning at 230/250 °C. As a result, neither succinic nor maleic anhydride modified AHL yielded spinnable fibers. Gauged from the spinning process alone, it would seem that acetic and phthalic anhydride modifications are the preferable modifications for AHL.

The use of softwood lignin as a precursor would further decrease the cost and precursor supply strain of carbon fiber production.[36,37] However, softwood lignins are subject to a higher degree of polymeric cross-linking than hardwood lignins.[34−37] This property hampers thermal mobility of softwood lignin polymer backbone and charring occurs before melt extrusion can be achieved, effectively limiting the use of softwood lignin as a precursor. However, in the present study, acid anhydride modified Kraft softwood lignin was successfully spun into fine, flexible fibers in the 190/215 °C to 195/220 °C range before oxidation occurred at 200/225 °C. Reaction of hydroxyl groups with the acid anhydride effectively reduced the cross-linking tendency of Kraft softwood lignin and thus lowered the melting point below the temperature for charring.

Thermostabilization and Carbonization. Lignin fibers were thermally stabilized to cross-link the polymer and release residual volatile components. Oxidative stabilization prevents the lignin fiber from sticking, shrinking, or melting during the subsequent carbonization process.[2,38,39] Alternatively, thermal stabilization can also be used to achieve controlled fiber−fiber fusion and facilitates processing of fibers into fused carbon fiber mats.[22]

The subsequent carbonization under an inert atmosphere involves dehydration and decarboxylation reactions in combination with condensation and aromatization releasing most of the noncarbon elements.[40] The resulting carbon fiber consists of graphitic domains embedded in an amorphous carbon matrix.

Characterization of Lignin Carbon Fibers by Neutron Diffraction. The reduced atomic pair distribution functions (PDF) represents the probability of finding an atom at a distance r from a reference atom.

$$G(r) = 4\pi r[\rho(r) - \rho_0] \quad (1)$$

Where $\rho(r)$ is the pair density at the distance r and ρ_0 is average atomic number density. Experimentally, $G(r)$ can be obtained by Fourier transformation of the total neutron scattering structure factor $S(Q)$:

$$G(r) = \frac{2}{\pi}\int_0^\infty Q[S(Q) - 1]\sin(Qr)\, dQ \quad (2)$$

where Q is the elastic scattering vector $Q = 4\pi \sin(\theta)/\lambda$ with 2θ defined as the scattering angle and λ as the wavelength of the radiation used. As $S(Q)$ is derived from the total coherent scattering intensity, both Bragg scattering and diffuse scattering contribute to the PDF. Therefore, the PDF method is suitable for the characterization of materials with well-ordered local structures, but limited structural coherence beyond the nanometer length scale.[41] The PDFs show that the choice of precursor modification has little effect on the microstructure of lignin carbon fibers after carbonization (Figure 5). PDFs in all four cases have similar patterns and present peaks corresponding to similar interatomic distances (Table 3). The first peak in all five curves appears at 1.41 Å and matches the in plane C−C bond distance in graphite. The second and third peaks in all samples appear at 2.45 and 2.84 Å. These values match the in-plane distances to the next-nearest neighbor and third closest neighbor in hexagonal aromatic rings of graphite (1.41, 2.47, and 2.85 Å). The fourth peak corresponds to the spacing between nearest carbon atoms on adjacent graphene sheets with a distance of 3.73 Å (3.75 Å in carbon fibers from modified precursors). All subsequent peaks arise from long-range correlations. The intensity of peaks decays rapidly with interatomic separation revealing a much shorter range of structural coherence compared to crystalline graphite. The difference between PDFs of carbon fibers obtained from modified and unmodified lignins is small indicating that the size of graphitic domains and the volume fraction of amorphous carbon are not strongly perturbed by the lignin precursor chemistry. Although esterification with acid anhydrides is shown to effectively modify the functional groups resulting in improved processability of the lignin, chemical modification preserves the molecular integrity of the biopolymer backbone and does not impair the formation of nanoscale graphitic domains. X-ray diffraction data of AHL lignin carbon fibers[42−44] has been reported in one of our recent publications.[22] All observed reflections are broad indicating extremely small crystalline sizes. Analysis of the (002) reflection indicates minimal crystallite sized of 0.9, 1.2, and 1.4 nm for carbonization temperatures of 1000, 1500, and 2000 °C, respectively. It can be concluded that the material contains a high level of lattice defects and distortions between graphitic basal planes and no preferential orientation along the fiber axis.

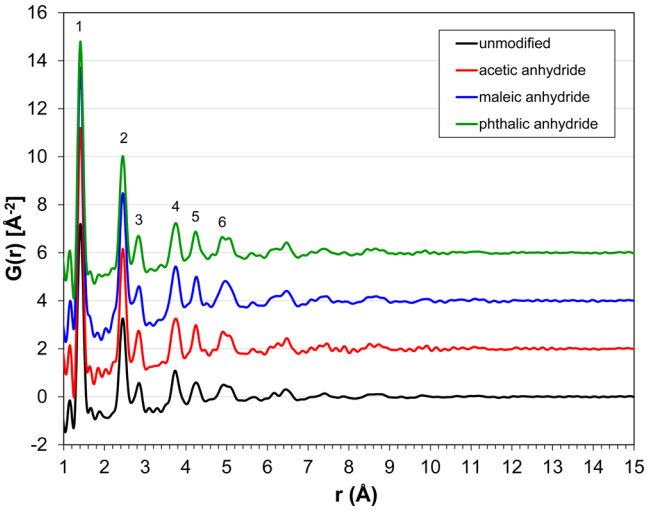

Figure 5. Experimental neutron PDF data obtained from Alcell hardwood with variable precursor treatments. PDFs are progressively shifted along the ordinate by units of 2 relative to the PDF of unmodified LCF. The first six peaks are numbered and the corresponding real space distances are listed in Table 3.

Table 3. Real Space Distances for the First Six Peaks Derived from PDFs in Figure 5

peak no.	r [Å]			
	unmodified	acetic anhydride	maleic anhydride	phthalic anhydride
1	1.41	1.41	1.41	1.41
2	2.45	2.45	2.45	2.45
3	2.85	2.84	2.85	2.83
4	3.73	3.75	3.75	3.75
5	4.25	4.24	4.26	4.24
6	4.92	4.91	4.97	4.89

Scanning Electron Microscopy (SEM). SEM images obtained from lignin carbon fibers (Figure 6) show that nearly every fiber cross section displayed a cylindrical hollow void, coincident with the fiber's axial direction with a diameter of 10−25 μm. Oxidative stabilization may have effectively cross-linked the polymers only to a certain depth from the surface, beyond which diffusion of oxygen was limited and thus did not induce cross-linking. During carbonization, the formation of voids leads to structural imperfections on the micron scale. Although these voids clearly result in inferior tensile and shear strengths, the increased microscale porosity could both increase the interface with a liquid electrolyte and ion diffusion rates. Fully immersed in the electrolyte, stable graphitic structures

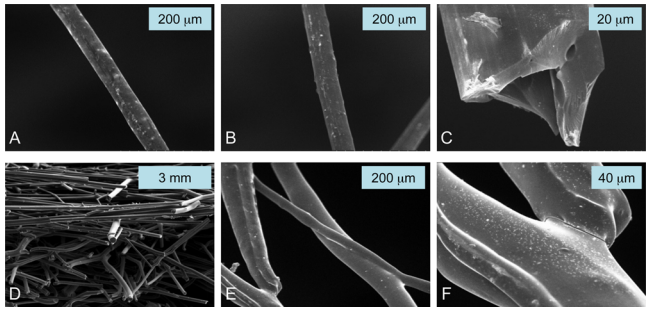

Figure 6. Scanning electron microscope (SEM) images of lignin carbon fibers. (A) Unmodified Alcell hardwood lignin (AHL); (B) phthalic anhydride modified AHL; (C) close-up and cross section of a phthalic anhydride modified AHL based carbon fiber with a hollow center; (D) fused lignin carbon fiber mat (AHL); (E, F) examples of fiber−fiber fusion in phthalic anhydride modified Kraft softwood lignin (KSL).

dx.doi.org/10.1021/sc500189p | ACS Sustainable Chem. Eng. 2014, 2, 2002−2010

embedded in a porous amorphous carbon matrix promote resistance to exfoliation and facilitates rapid exchange of lithium ions between the electrolyte and the graphitic carbon of the anode. Thus, anode porosity can serve as an indicator for the underlying carbon microstructure. We previously reported BET surface areas, pore volumes, and SEM surface morphology of these lignin carbon fibers.[18] Although the surface areas are comparable to commercial graphitic carbon materials, chemical modification of the lignin precursors appears to promote a heightened degree of submicron porosity. Acetic anhydride and phthalic anhydride modified AHL showed surface areas that were approximately four times higher compared to unmodified AHL.[18]

Resistivity Measurements. According to Ohm's law, $V = IR$, where V corresponds to the voltage across the resistance of that length of the fiber, I is the current, and R is the resistance of the fiber. In the experiment, voltage across the resistance of that length of the fiber is calculated. Then, using the fiber radius (r), the distance between the voltage probes (d), and the above information, the material's resistivity is given by $\rho = Rr^2\pi/d$. There was no significant difference in the resistivities of fibers prepared from different precursors. All fiber samples exhibited resistivities in the range between 1×10^{-5} and 1×10^{-4} Ω·m with an average value of $1.49 \times 10^{-4} \pm 1.09 \times 10^{-4}$ Ω·m (standard deviation, $n = 4$). For comparison, the resistivity of copper is 1.72×10^{-8} Ω·m,[38,45] and typical values for graphite range between 3×10^{-5} and 6×10^{-4} Ω·m depending on the presence of impurities.[45] The electrochemical performance of AHL carbon fibers in monolithic Li-ion battery electrodes has been characterized in detail.[22]

CONCLUSIONS

Lignin carbon fibers were prepared from unmodified and acid anhydride modified Alcell hardwood and softwood lignin precursors. The precursor materials were melt-processed into lignin fibers and optimal extrusion parameters were determined for each type of lignin precursor. Interestingly, although melt processing of softwood lignins is generally considered not feasible, modification of Kraft softwood lignin with phthalic or acetic anhydride resulted in a precursor that could be melt extruded and spun into fibers. Analysis of the precursors by FT-ICR MS reveals distinct differences in the chemical composition of softwood and hardwood lignin and as a result of chemical modifications. A comparison of heteroatom class distributions shows that chemical modification of Kraft softwood lignin results in a mass distribution similar to Alcell hardwood lignin. All lignin fibers were oxidatively stabilized and carbonized under similar conditions. The SEM characterization of lignin carbon fiber samples revealed fibers with a hollow center and a microporous surface morphology. The hollow cores and disordered microstructures result in the low mechanical strength of these fibers. However, the large voids increase the interface between the electrolyte and the anode material. Moreover, the highly disordered microstructure limits exfoliation of graphite due to cointercalation and solid-electrolyte interphase (SEI) formation and enable the use of polycarbonate electrolytes.[22] Furthermore, we provide PDF data from neutron diffraction experiments for lignin carbon fibers derived from different precursors. All $G(r)$ functions show interatomic correlation peaks corresponding to characteristic distances in graphite. However, the $G(r)$ functions decay rapidly with increasing distance, which is consistent with nanometer graphitic domains embedded in an amorphous matrix. A comparison of all PDFs shows that the chemistry of the precursor has little impact on the carbon structure. Thus, we conclude that chemical modification does not interfere with the development of a unique carbon mesostructure during carbonization. Resistance measurements confirm that despite their limited crystallinity, the carbon fibers exhibit resistivity comparable to typical values for graphite. The combination of innovative melt-processing techniques enabling the production of fused carbon fiber mats, a unique carbon mesostructure and graphite-like electrical properties make lignin-based carbon fibers a viable alternative to conventional anode materials in Li-ion or Na-ion batteries.

AUTHOR INFORMATION

Corresponding Authors

*Phone: 1(865)574 7444. Fax: +1(865) 576 8646 E-mail: johsa@ornl.gov (A.J.).

*E-mail: chatterjees@ornl.gov (S.C.).

Funding

This research was supported by the Laboratory Directed Research and Development Program of the Oak Ridge National Laboratory (ORNL). ORNL is managed by UT-Battelle, LLC, for the U.S. Department of Energy under contract No. DE-AC05-00OR22725.

Notes

The authors declare no competing financial interest.

ACKNOWLEDGMENTS

Work performed at the National High Magnetic Field Laboratory was supported by the National Science Foundation (NSF), Division of Materials Research through DMR-1157490, Florida State University, the Future Fuels Institute, BP/The Gulf of Mexico Research Initiative to the Deep-C Consortium, and the State of Florida. Neutron diffraction experiments were performed on the Nanoscale-Ordered Materials Diffractometer (NOMAD) at Oak Ridge National Laboratory's Spallation Neutron Source supported by the Scientific User Facility Division, Office of Basic Energy Sciences, U.S. Department of Energy.

ABBREVIATIONS

PAN, polyacrylonitrile
H, *p*-coumaryl
G, coniferyl
S, sinapyl
THF, tetrahydrofuran
MeOH, methanol
AHL, Alcell hardwood lignin
KSL, Kraft softwood lignin
T_g, glass transition temperature
T_m, melting temperature
FT-ICR MS, Fourier-transform ion cyclotron resonance mass spectrometry
ESI, electrospray ionization
IUPAC, International Union of Pure and Applied Chemistry
LME, laboratory mixing extruder
TUS, take-up system
NOMAD, Nanoscale-Ordered Materials Diffractometer
SNS, Spallation Neutron Source
SEM, scanning electron microscopy
PDF, pair distribution function

REFERENCES

(1) Huang, X. Fabrication and properties of carbon fibers. *Materials* **2009**, *2*, 2369−2403.

(2) Chung, D. L. *Carbon Fiber Composites*; Butterworth-Heinemann: New York, 1994.

(3) Zakzeski, J.; Bruijnincx, P. C. A.; Jongerius, A. L.; Weckhuysen, B. M. The Catalytic Valorization of Lignin for the Production of Renewable Chemicals. *Chem. Rev.* **2010**, *110*, 3552−3599.

(4) Saito, T.; Brown, R. H.; Hunt, M. A.; Pickel, D. L.; Pickel, J. M.; Messman, J. M.; Baker, F. S.; Keller, M.; Naskar, A. K. Turning renewable resources into value-added polymer: development of lignin-based thermoplastic. *Green Chem.* **2012**, *14*, 3295−3303.

(5) Luo, J.; Genco, J.; Cole, B.; Fort, R. Lignin Recovered from the Near-Neutral Hemicellulose Extraction Process as a Precursor for Carbon Fiber. *BioResources* **2011**, *6*, 4566−4593.

(6) Harton, S. E.; Pingali, S. V.; Nunnery, G. A.; Baker, D. A.; Walker, S. H.; Muddiman, D. C.; Koga, T.; Rials, T. G.; Urban, V. S.; Langan, P. Evidence for Complex Molecular Architectures for Solvent-Extracted Lignins. *ACS Macro Lett.* **2012**, *1*, 568−573.

(7) Baker, D. A.; Gallego, N. C.; Baker, F. S. On the characterization and spinning of an organic-purified lignin toward the manufacture of low-cost carbon fiber. *J. Appl. Polym. Sci.* **2012**, *124*, 227−234.

(8) London Metal Exchange, MetalPrices, Copper. http://www.metalprices.com/metal/copper/lme-copper-cash-official (accessed Jan 9, 2014).

(9) Isaev, I.; Salitra, G.; Soffer, A.; Cohen, Y. S.; Aurbach, D.; Fischer, J. A new approach for the preparation of anodes for Li-ion batteries based on activated hard carbon cloth with pore design. *J. Power Sources* **2003**, *119−121*, 28−33.

(10) Han, Y. S.; Yu, J. S.; Park, G. S.; Lee, J. Y. Effects of Synthesis Temperature on the Electrochemical Characteristics of Pyrolytic Carbon for Anodes of Lithium-Ion Secondary Batteries. *J. Electrochem. Soc.* **1999**, *146*, 3999−4004.

(11) Takami, N.; Satoh, A.; Hara, M.; Ohsaki, T. Structural and Kinetic Characterization of Lithium Intercalation into Carbon Anodes for Secondary Lithium Batteries. *J. Electrochem. Soc.* **1995**, *142*, 371−379.

(12) Stane-Pejovnik, M. B.; Dominko, R.; Drofenik, J.; Gaberscek, M. Use of Materials Science Principles in Battery Design: Gelatin in Lithium Batteries. *Acta Chim. Slov.* **2001**, *48*, 115−125.

(13) Fey, G. T. K.; Cho, Y. D.; Chen, C. L.; Huang, K. P.; Lin, Y. C.; Kumar, T. P.; Chan, S. H. Pyrolytic Carbons from Progen-treated Rice Husk as Lithium-insertion Anode Materials. *Int. J. Chem. Eng. Appl.* **2011**, *2*, 20−25.

(14) Sheng Su, D.; Schlögl, R. Nanostructured carbon and carbon nanocomposites for electrochemical energy storage applications. *ChemSusChem* **2010**, *3*, 136−138.

(15) Zhai, Y.; Dou, Y.; Zhao, Z.; Fulvio, P. F.; Mayes, R. T.; Dai, S. Carbon materials for chemical capacitive energy storage. *Adv. Mater.* **2011**, *23*, 4828−4850.

(16) Guo, B.; Wang, X.; Fulvio, P. F.; Chi, M.; Mahurin, S. M.; Sun, X.-G.; Dai, S. Soft-Templated mesoporous carbon-carbon nanotube composites for high performance lithium-ion batteries. *Adv. Mater.* **2011**, 1−6.

(17) Ding, J.; Wang, H.; Li, Z.; Kohandehghan, A.; Cui, K.; Xu, Z.; Zahiri, B.; Tan, X.; Memarzadeh Lotfabad, E.; Olsen, B. C.; Mitlin, D. Carbon nanosheet frameworks derived from Peat Moss as high performance sodium ion battery anodes. *ACS Nano* **2013**, *7*, 11004−11015.

(18) Chatterjee, S.; Clingenpeel, A.; McKenna, A.; Rios, O.; Johs, A. Synthesis and characterization of lignin-based carbons for energy storage applications. *RSC Adv.* **2014**, *4*, 4743−4753.

(19) Sarkanen, S.; Teller, D. C.; Hall, J.; McCarthy, J. L. Lignin. 18. Associative effects among organosolv lignin components. *Macromolecules* **1981**, *14*, 426−434.

(20) Foston, M.; Nunnery, G. A.; Meng, X.; Sun, Q.; Baker, F. S.; Ragauskas, A. NMR - A critical tool to study the production of carbon fiber from lignin. *Carbon* **2013**, *52*, 65−73.

(21) Luo, J.; Genco, J.; Cole, B.; Fort, R. Lignin recovered from the near-neutral hemicellulose extraction process as a precursor for carbon fiber. *BioResources* **2011**, *6*, 4566−4605.

(22) Tenhaeff, W. E.; Rios, O.; More, K.; McGuire, M. A. Highly Robust Lithium Ion Battery Anodes from Lignin: An Abundant, Renewable, and Low-Cost Material. *Adv. Funct. Mater.* **2013**, DOI: 10.1002/adfm.201301420.

(23) Baker, F. S.; Baker, D. A.; Menchhofer, P. A. Carbon nanotube(CNT)-enhanced precursor for carbon fiber production and method of making a CNT-enhanced continuous lignin fiber. U.S. patent US 20110285049 A1 20111124, 2011.

(24) Podgorski, D. C.; McKenna, A. M.; Rodgers, R. P.; Marshall, A. G.; Cooper, W. T. Selective Ionization of Dissolved Organic Nitrogen by Positive Ion Atmospheric Pressure Photoionization Coupled with Fourier Transform Ion Cyclotron Resonance Mass Spectrometry. *Anal. Chem.* **2012**, *84*, 5085−5090.

(25) Kaiser, N.; Quinn, J.; Blakney, G.; Hendrickson, C.; Marshall, A. A Novel 9.4 T FT-ICR Mass Spectrometer with Improved Sensitivity, Mass Resolution, and Mass Range. *J. Am. Soc. Mass Spectrom.* **2011**, *22*, 1343−1351.

(26) Blakney, G. T.; Hendrickson, C. L.; Marshall, A. G. Predator data station: A fast data acquisition system for advanced FT-ICR MS experiments. *Int. J. Mass Spectrom.* **2011**, *306*, 246−252.

(27) Xian, F.; Hendrickson, C. L.; Marshall, A. G. High Resolution Mass Spectrometry. *Anal. Chem.* **2012**, *84*, 708−719.

(28) Savory, J. J.; Kaiser, N. K.; McKenna, A. M.; Xian, F.; Blakney, G. T.; Rodgers, R. P.; Hendrickson, C. L.; Marshall, A. G. Parts-Per-Billion Fourier Transform Ion Cyclotron Resonance Mass Measurement Accuracy with a "Walking" Calibration Equation. *Anal. Chem.* **2011**, *83*, 1732−1736.

(29) Kendrick, E. A Mass Scale Based on CH2 = 14.0000 for High Resolution Mass Spectrometry of Organic Compounds. *Anal. Chem.* **1963**, *35*, 2146−2154.

(30) Hughey, C. A.; Hendrickson, C. L.; Rodgers, R. P.; Marshall, A. G.; Qian, K. Kendrick Mass Defect Spectrum: A Compact Visual Analysis for Ultrahigh-Resolution Broadband Mass Spectra. *Anal. Chem.* **2001**, *73*, 4676−4681.

(31) D'Auria, M.; Emanuele, L.; Racioppi, R. FT-ICR-MS analysis of lignin. *Nat. Prod. Res.* **2012**, *26*, 1368−1374.

(32) D'Auria, M.; Emanuele, L.; Racioppi, R. A FT-ICR MS study of lignin: determination of an unusual structural repetitive unit in steam exploded lignin from wheat straw. *Lett. Org. Chem.* **2011**, *8*, 436−446.

(33) Kim, S.; Kramer, R. W.; Hatcher, P. G. Graphical Method for Analysis of Ultrahigh-Resolution Broadband Mass Spectra of Natural Organic Matter, the Van Krevelen Diagram. *Anal. Chem.* **2003**, *75*, 5336−5344.

(34) Kadla, J. F.; Kubo, S.; Venditti, R. A.; Gilbert, R. D.; Compere, A. L.; Griffith, W. Lignin-based carbon fibers for composite fiber applications. *Carbon* **2002**, *40*, 2913−2920.

(35) Luo, J. *Lignin-Based Carbon Fiber*; M.S. Thesis, The University of Maine, 2010.

(36) Eckert, R. C.; Abdullah, Z. Carbon fibers from kraft softwood lignin. US Patent 7,794,824, 2010.

(37) Zhang, M.; Ogale, A. A. Carbon fibers from dry-spinning of acetylated softwood kraft lignin. *Carbon* **2014**, *69*, 626−629.

(38) Braun, J. L.; Holtman, K. M.; Kadla, J. F. Lignin-based carbon fibers: Oxidative thermostabilization of kraft lignin. *Carbon* **2005**, *43*, 385−394.

(39) Edie, D. D. The effect of processing on the structure and properties of carbon fibers. *Carbon* **1998**, *36*, 345−362.

(40) Funke, A.; Ziegler, F. Hydrothermal carbonization of biomass: A summary and discussion of chemical mechanisms for process engineering. *Biofuel Bioprod. Bior.* **2010**, *4*, 160−177.

(41) Proffen, T.; Billinge, S. J. L.; Egami, T.; Louca, D. Structural analysis of complex materials using the atomic pair distribution function - a practical guide. *Z. Kristallogr.* **2003**, *218*, 132−143.

(42) Alexander, L. E. *X-ray diffraction methods in polymer science*; Wiley-Interscience: New York, 1969.

(43) Warren, B. E.; Bodenstein, P. The diffraction pattern of fine particle carbon black. *Acta Crystallogr.* **1965**, *18*, 282−286.
(44) Warren, B. E.; Bodenstein, P. The Shape of Two-Dimensional Carbon Black Reflections. *Acta Crystallogr.* **1966**, *20*, 602−605.
(45) Giancoli, D. C. *Physics*, 4th ed.; Prentice Hall, 1995.